TOC Figure

In contrast to the case of carbon nanotubes, the negative strain energy indicates that single-walled and double-walled triazine-based carbon nitride nanotubes (TACNNTs) are appreciably more stable than thesingle layer and the bilayer of g^t-C_3N_4, respectively.The band gap of (10,0)@(20,0) TACNNTs is appreciably smaller than those of constituent SWCNNTs. Boron-doping turns the material into a magnetic semiconductor.

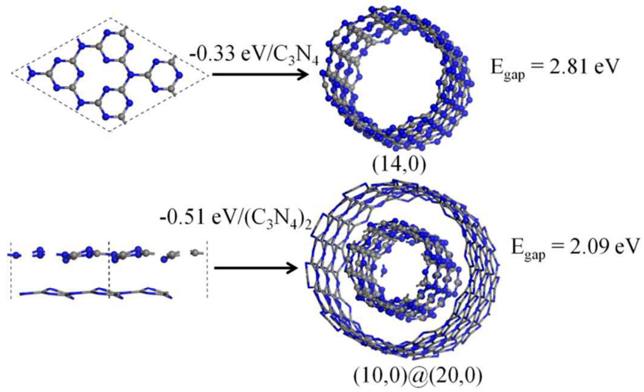

Stability and Electronic Structures of Triazine-Based Carbon Nitride Nanotubes

Fazel Shojaei[1]

[1]Department of Chemistry and Bioactive Material Sciences and Research Institute of Physics and Chemistry, Jeonbuk National University, Chonju, Chonbuk 561-756, Republic of Korea

and

Hong Seok Kang[2,*]

[2]Department of Nano and Advanced Materials, College of Engineering, Jeonju University, Hyoja-dong, Wansan-ku, Chonju,Chonbuk 560-759, Republic of Korea

*Corresponding author: hsk@jj.ac.kr

ABSTRACT

We investigate the possibility of forming single-walled (SWTACNNTs) and double-walled carbon nitride nanotubes (DWTACNNTs) from triazine-based C_3N_4 sheets (g^t-C_3N_4) that have been synthesized recently, using calculations based on the density functional theory. In contrast to the case of single-walled carbon nanotube, the negative strain energy indicates that SWTACNNTs are appreciably more stable than a single sheet of g^t-C_3N_4. In addition, the SWTACNNTs are chirality-specific semiconductors. Boron doping at a carbon site turns (14,0) SWTACNNT into a magnetic semiconductor, where adjacent *p*-magnetic centers strongly couple ferromagnetically. Phosphorus doping at a nitrogen site decreases the band gap by more than 0.28 eV. DWTACNNTs are not only more stable than constituent SWTACNNTs but also appreciably more stable than g^t-C_3N_4 bilayer. The band gap of (10,0)@(20,0) TACNNT is more than 0.48 eV smaller than those of the constituent SWTACNNTs.

1. INTRODUCTION

Binary carbon nitrides are a class of sustainable materials consisting of carbon and nitrogen, only. Motivated by theoretical calculations that predicted a very large bulk modulus for diamond-like β-C_3N_4,[1] carbon nitride materials have received a great deal of attention in the last few decades.[2-6] Focusing on the layered carbon nitride materials, many different architectures including carbon nitride nanotubes (CNNTs),[3] nano-onions,[4] and graphitic carbon nitrides (g-C_3N_4 and g-C_4N_3)[5,6] have been successfully fabricated. These allotropes exhibit different C/N ratios as well as different electronic and chemical properties.

Under ambient conditions, heptazine-based g-C_3N_4 (g^h-C_3N_4) is regarded as one of the most stable allotropes of graphitic carbon nitride materials.[7] Its basic building block is a heptazine unit (C_6N_7). The material can be synthesized by the polymerization of cyanamide or dicyandiamide.[8] In recent years, the material has been found to have promising applications in heterogeneous catalysis,[9] metal-free photocatalysis,[10-15] energy conversion,[16] and bio imaging[17]. Particular attention has been drawn to using it as an efficient photocatalyst for hydrogen generation under visible light irradiation, in view of its band gap (= 2.75 eV) corresponding to blue light.[18] g^h-C_3N_4 has also been successfully doped with carbon, boron, fluorine, phosphorus, and sulfur.[16] As an example, Yan et al. found that the boron doping results in a reduced band gap (2.66eV) and a higher activity for the photodegradation of some dyes.[19]

Motivated by the unusual properties of carbon nanotubes (CNTs), many efforts have been devoted to the synthesis CNNTs. As in g^h-C_3N_4, most (HACNNTs) of them have been found to have heptazine as a basic building unit.[3,20,21] It exhibits a strong photoluminescence at 460 nm.[3] In addition, it shows much higher photocatalytic activity for the degradation of organic dyes than g^h-C_3N_4.[3] A theoretical calculation shows that their optical properties are independent of the chirality.[22]

Very recently, a different allotrope (= g^t-C_3N_4) of layered g^h-C_3N_4 with the same C_3N_4

stoichiometry was successfully synthesized using an ionothermal interfacial reaction.[23] The basic building block of the historical material is a triazine unit (C_3N_3) instead of a heptazine unit (C_6N_7).[1] The allotrope is also a porous material in which a vacancy site consists of one missing atom instead of four. This report is unexpected, because its *single* sheet has been known to be appreciably less stable than the aforementioned g^h-C_3N_4.[7,22] The g^t-C_3N_4 was shown to be cleaved down to approximately three layers, for which the UV/VIS spectrum indicates that its optical gap is less than 1.6 eV.[23] Therefore, it would be quite valuable to investigate if the material can roll up to form triazine-based carbon nitride nanotubes (TACNNTs). A preliminary calculation using the tight-binding method showed that the zigzag TACNNTs (*z*TACNNTs) are more stable than armchair TACNNTs (*a*TACNNTs).[24] This observation needs a careful reconsideration, because their observation was based on the extended Huckel approximation in which structure relaxation was not performed. Other than that, theoretical calculations on the tubes are quite rare, particularly on their electronic structures.

In this work, we will do a systematic investigation on the stability of TACNNTs in comparison with that of CNTs. In addition, we will also investigate their electronic structures and doping effects. Furthermore, we will study the possibility of forming double-walled TACNNTs (DWTACNNTs) as well as their electronic structures. This is because the TACNNTs may exist in the form of multi-walled tubes rather than in the form of single-walled tubes. In fact, Guo et al. previously synthesized multi-walled nanotubes with C_3N_4 stoichiometry.[25]

2. THEORETICAL METHODS

Geometry optimizations are performed using the Vienna ab-initio simulation package (VASP)[26,27] Electron-ion interactions are described by the projector-augmented wave (PAW) method, which is primarily a frozen-core all-electron calculation.[28] For structure optimization, atoms are relaxed in the direction of the Hellmann-Feynman force using the conjugate gradient method until a stringent convergence criterion (= 0.03 eV/Å) is satisfied. When necessary, spin-polarized calculations are also performed to check whether there is any magnetization in the systems.

For single-walled TACNNTs (SWTACNNTs), all the results rely on the PBE exchange-correlation function. On the one hand, the local density approximation (LDA) is employed for the DWTACNNTs. This is because the PBE fails to describe systems dominated by van der Waals interaction, while the LDA is known to describe the interaction in the geometric and electronic structures consistently. In the LDA calculation, we reoptimize the lattice constant and the geometry of the system of interest. When necessary, the LDA calculation is complemented by the PBE-D2 calculation which represents the PBE that empirically incorporates van der Waals interaction using Grimme′s approach.[29]

To simulate a 2D sheet of g^t-C_3N_4, we employ a hexagonal primitive cell. The PBE-optimized lattice constant is 4.72 Å. We keep the vacuum space along the direction normal to the sheet plane large enough (= 15 Å) to guarantee no appreciable interaction between two adjacent layers. k-point sampling is performed using $19\times19\times1$ points. To simulate TACNNTs, vacuum space is also introduced along two (= Y and Z) directions normal to the tube (= X) axis. k-point sampling is done using $19\times1\times1$ and $11\times1\times1$ points for aTACNNTs and zTACNNTs, respectively.

3. RESULTS AND DISCUSSION

First, we will investigate the tendency of the g^t-C_3N_4 to form tubular structures. Before going into any detail, we want to note that only even-numbered n values (n = 2m) are allowed for the TACNNTs. This is because the chiral index (n,m) of a tube is defined based on the primitive vectors of graphene, not on those of the g^t-C_3N_4 which consists of 2×2 cells of graphene. In this respect, we recall that Enyashin and Ivanovskii's chiral index (n',m') of a TACNNT is equivalent to ($2n'$, $2m'$) in our case.[24] We believe that our definition is less confusing, when we want to compare physical properties of TACNNTs with those of CNTs.

Table 1 shows the strain energy (E_{st}) of *a*TACNNTs with various chiral indices n obtained from the PBE calculation. Here, E_{st} is defined as the total energy per C_3N_4 unit for the (n,n) TACNNT minus that for the g^t-C_3N_4. The E_{st} data show that all the TACNNTs are energetically more stable than the 2D g^t-C_3N_4, except for (4,4) TACNNT which has the smallest diameter. This observation indicates that the tube formation does not introduce strain but releases it. This observation is in strong contrast with the case of armchair CNTs (*a*CNTs), for which the E_{st} data are all positive irrespective of the diameter of the tube. Therefore, we conjecture that it is much easier to synthesis the TACNNTs than the CNTs from their respective 2D sheets. In addition, Table 1 and Figure 1 show that (14,14) TACNNT is the most stable among all *a*TACNNTs investigated. This observation is different from the case of the *a*CNT in which its stability increases monotonically with the diameter. Therefore, (14,14) TACNNT would be produced the most among all *a*TACNNTs, while larger and larger diameters are preferred in the case of *a*CNTs.

The pronounced stability of *a*TACNNTs over the g^t-C_3N_4 can be ascribed to the effective release of repulsion between lone-pair electrons belonging to the adjacent nitrogen atoms around a vacancy site. Table 1 shows that this is indeed the case. In order to understand this better, we describe the geometrical feature of *a*TACNNTs. Figure 2 shows four kinds of nitrogen atoms. The graphitic nitrogen (N_g) has two π electrons oriented perpendicular to the tube surface. On the one hand, a pyridinelike (N_p) nitrogen atom is characterized by two lone-pair electrons lying nearly parallel to the tube surface. It can be further divided into two groups. In the N_p^o groups, the nitrogen atom protrudes from the surface of the tube and defines the outer diameter of the tube. Likewise, in the N_p^i group, the nitrogen atom sinks into the tube and defines the inner diameter of the tube. Meanwhile, N_g atoms are located between N_p^o and N_p^i atoms along the radial direction. We find that N_g: N_p^i: N_p^o =1: 1: 2. Two of the three N_p atoms around one vacancy site belong to group N_p^o, which can be further divided into N_p^{o1} and N_p^{o2} atoms. The remaining one belongs to group N_p^i. Table 1 shows that all three kinds of N-N distances ($l_{N\text{-}N}$) involving N_p^i and N_p^o atoms are larger than the corresponding distances in the g^t-C_3N_4.

Figure S1 compares the diameter of *a*TACNNT with that of *a*CNT of the same chiral index *n*. Overall, the outer diameters of *a*TACNNTs are close to those of the corresponding CNTs, while the inner diameters are appreciably smaller. The lattice constants are also smaller than the corresponding data (2.47×2 = 4.94 Å) for *a*CNTs by 0.16~0.26 Å. All these observations can be ascribed to the corrugation of the tube surface.

Next, we investigate the electronic structures of *a*TACNNTs. The PBE band structures of (8,8) and (14,14) TACNNTs shown in Figure S2 indicate that both of them are semiconductors. Irrespective of the chiral index, subbands around the valence band basically represent σ states originating from the lone-pair states of the nitrogen atoms, while another subbands around the conduction band represent π^* states. As shown in Table 1, band gaps of the two tubes are indirect and amount to 2.64 and 2.62 eV, respectively. The optical gaps are similar to the band gaps, because the $\Gamma \rightarrow \Gamma$ transitions in Table 1 occur at similar energies. The table also shows that all the *a*TACNNTs investigated are semiconductors with similar band gaps. Except for (4,4) TACNNT, the band gaps are slightly larger than that (= 2.38 eV) of a *single* sheet of g^t-C_3N_4 due to the quantum confinement effect along the tube diameter.

Henceforth, we investigate the E_{st} of *z*TACNNTs with various chiral indices *n* using the PBE calculation. Table 2 shows that the *z*TACNNTs are much more stable than the g^t-C_3N_4. A comparison with the case of *a*TACNNTs shows that the *z*TACNNTs are substantially more stable than those with similar diameters. For example, Tables 1 and 2 show that the E_{st} values are -0.33 and -0.16 eV per C_3N_4 unit for (14,0) and (8,8) TACNNTs, respectively. Therefore, we can conclude that *z*TACNNTs are almost exclusively produced when TACNNTs are generated. As shown in Figure 1, this is quite different from the case of CNTs in which the strain energy is almost independent of the chirality of the tube. For example, the figure shows that E_{st} values are 0.46 eV per C_7 unit for both (14,0) and (8,8) CNTs, respectively.

In addition, the table shows that (14,0) TACNNT is the most stable among all *z*TACNNTs investigated. The TACNNT becomes progressively less stable as the diameter becomes larger, as shown in Figure 1. The pronounced stability of the *z*TACNNTs over the *a*TACNNTs is partly shown in the N_p^{o1}-N_p^{i} and N_p^{o1}-N_p^{o2} distances which are larger than those for the *a*TACNNTs, where three kinds of N atoms are defined in Figure 3.

Here, we describe the geometrical features of *z*TACNNTs shown in Figure 3. First, the ratio, N_g: N_p^{i}: N_p^{o} =1: 1: 2, still holds. For (14,0) TACNNT, the lattice constant is smaller than that of (14,0) CNT by 7%. The decrease is larger than those for *a*TACNNTs. For example, the decrease is 5% for (14,14) TACNNT. In short, there is a larger contraction of *z*TACNNTs along the tube direction than *a*TACNNTs. In Figure 3, this effect is clearly shown in the contraction of the axial C-N_g distance (= 1.40 Å) parallel to the tube (= X) axis. The bond length is shorter than the other two C-N_g distances (= 1.44 Å) around the same N_g atom, because the non-axial bonds are oriented at 60^o with respect to the tube axis. Obviously, this kind of disproportionation is not observed in *a*TACNNTs, because there are no axial C-N_g bonds in the tubes.

Now, we describe the PBE band structures of *z*TACNNTs. Figure 4 shows that both (14,0) and (24,0) TACNNTs are semiconductors. Similar to the case of *a*TACNNTs, the valence band represents σ states originating from the lone-pair states of the nitrogen atoms, while the conduction band represents π^* states. [There should be a certain degree of $\sigma-\pi$ hybridizations in both bands due to the curvature of the tubes.] This is also the case for other *z*TACNNTs investigated. The band gaps of (8,0) ~ (20,0) TACNNTs are larger than those of *a*TACNNTs with similar diameters. On the other hand, the gaps are independent of the chirality, when the diameters are larger. In fact, the band gaps of (24,0) and (28,0) TACNNTs are almost the same as those of (14,14) and (16,16) TACNNTs, respectively, being also larger than that (= 2.38 eV) of a *single* sheet of g^t-C_3N_4.

Next, we investigate the effect of phosphorus doping on the geometrical and electronic structures of *z*TACNNTs using the PBE calculation. We recall that the P-doping on the g^h-C_3N_4 was recently realized experimentally.[30] In order to do this, we first calculate the relative preference for the substitution of one P atom at each of the N_g, N_p^i, and N_p^o sites in (14,0) TACNNT. The P/N ratio is 1/56. Doping (P_g-doping) at an N_g site is the most stable, and doping (P_p^o-doping) at an N_p^o site is 0.08 eV less stable. However, the doping at an N_p^i site is impossible due to the severe steric hindrance. In the case of P_g-doping, the P atom protrudes from the tube surface by 0.46 Å, and the P_g-C bond lengths are 1.80 and 1.86 Å for an axial and two non-axial bonds, respectively. In the case of P_p^o-doping, the P atom protrudes from the tube surface by 0.83Å more than the case of N_p^o-doping, and the two P_p^o-C bond lengths are 1.77 Å.

Figure S3 shows the PBE band structures of P_g- and P_p^o-doped (14,0) TACNNTs, which are denoted as P_g- and P_p^o-(14,0) TACNNTs, respectively. The valence band represents localized σ states concentrated on a few atoms around the P atom, being separate from other delocalized subbands. On the one hand, the conduction band still represents delocalized π^* states. Consequently, the doping decreases the band gap of P_g-(14,0) TACNNT appreciably, i.e., from 2.81 eV to 2.53 eV for the $X \rightarrow \Gamma$ transition. In the case of the P_p^o-doping, the decrease is larger, i.e., from 2.81 eV to 2.32 eV. In short, the P-doping decreases the band gap of the TACNNT.

Now, we investigate the effect of boron doping on (14,0) TACNNT, which was also experimentally realized on the g^h-C_3N_4.[31] As shown in Figure 3, there are two kinds of carbon atoms, i.e., 21 C_1 and 21 C_2 atoms in a primitive cell. Our calculation of the relative doping preference for those two kinds of sites shows that a C_1 site is preferred to a C_2 site by 0.31 eV. Therefore, we can conclude that the doping will occur exclusively at C_1 sites. The B_{C1} doping turns the tube into a magnetic system of $1\,\mu_B$, where the spin polarization is mostly concentrated on two N_p atoms directly bonded to the B atom. The magnetic moments of two adjacent supercells couple ferromagnetically, as indicated by the energy difference (ΔE_{FM-NM}) of 0.17 eV between ferromagnetic (FM) and nonmagnetic (NM) states. Surprisingly, the FM state corresponds to a magnetic semiconductor with large exchange splitting, i.e., 0.81 ~ 0.90 eV depending upon *k*-state. In fact, Figure 5 shows that the band gap of the minority spin (= 0.64 eV) is significantly smaller than that (= 2.46 eV) of the majority spin which is comparable to that of the undoped TACNNT. Here, the splitted band (n = 224 in Figure 5) represents σ-states mainly derived from the lone-pair states of the two N_p atoms around the B atom. Therefore, the spin polarization can be mostly attributed to that of lone-pair electrons, not to the polarization of π electrons.

Herein, we delve into the possibility of forming DWTACNNTs. In order to do that, we consider (10,0)@(n,0) TACNNTs. For each of them, we take into account two different configurations shown in Figure 6. FF represents that both the inner and outer shells are oriented along the same direction. On the other hand, FR denotes that they are in *opposite* directions. In more detail, the inner shell of the FR configuration is rotated by 180° with respect to Y axis directed perpendicular to the tube axis. In each of FF and FR configurations, different initial structures, in which the inner shell is slid with respect to the outer one by different amounts, result in the same final structure after structure optimization. Our LDA calculation shows that the interwall binding energy (E_b) of the DWTACNNTs is -0.11 (-0.06), -0.16 (-0.15), and -0.07 (-0.07) eV per $(C_3N_4)_2$ unit for n = 18, 20, and 22, respectively. Here, the numbers outside and inside the parentheses denote E_b values for FR and FF configurations, respectively. The large binding energy leads us to conjecture that the TACNNTs may exist in the form of multi-walled tubes rather than in the form of single-walled tubes. In addition, the most stable inner-outer combination is (10,0)@(20,0) for the zigzag pairs investigated, whose stability is much more pronounced than adjacent combinations. This observation can be compared with the case of double-walled CNTs

(DWCNTs) in which the best combination was found to be (n,0)@(n+9,0).[32] In addition, the FR configuration is more stable than the FF configuration for all three pairs considered. However, the FF configuration is almost as stable as the FR configuration for (10,0)@(20,0) pairs. For the pair, a better estimation of the binding energy obtained from the PBE-D2 calculation is -0.24 eV and -0.23 eV for FR and FF configurations, respectively, being much larger than those from the LDA calculation. The binding is predominantly due to van der Waals interaction, as indicated by its contribution of -0.26 and -0.25 eV, respectively. We recall that the interwall binding energy is smaller than that (-0.31 eV) per C_{14} units of (10,0)@(19,0) CNT. Still, (10,0)@(20,0) TACNNT is much more stable than the bilayer of g^t-C_3N_4, as indicated by its negative strain energy (-0.51 eV) per $(C_3N_4)_2$ unit. Here, the strain energy of the double-walled tube is defined by the process: [the bilayer of g^t-C_3N_4]$\rightarrow$ (10,0)@(20,0) TACNNT. This value can also be compared to the corresponding datum (= 0.96 eV) for (10,0)@(19,0) CNT, which is still strongly positive.

Now, we describe the geometrical features of (10,0)@(20,0) TACNNT obtained from the PBE-D2 calculation. In Figure 6, the closest radial distances between the two shells, defined by the N_g atoms of the inner shell and N_p^i atoms of the outer shell, are 3.14 and 3.05 Å for FR and FF configurations, respectively. [Here, the radial distance corresponds to the interlayer distance along the radial direction.] The average radial distance, which is defined by the N_g atoms of the two shells, is 3.60 and 3.62 Å, respectively. It is worth mentioning that the distance is slightly larger than that (= 3.50 Å) in (10,0)@(19,0) CNT. These observations clearly indicate that the interwall interaction is mainly due to the van der Waals interaction. In both configurations, the outer diameters of the two shells match with each other along the tube axis.

Figure 7 shows the LDA band structures of (10,0)@(20,0) TACNNT. For both configurations, the valence band represents that of the (20,0) TACNNT, while the conduction band corresponds to that of (10,0) TACNNT. As a result, the band gaps are 2.09 and 2.13 eV for FR and FF configurations, respectively. They are appreciably smaller than the LDA band gaps of 2.73 and 2.62 eV for (10,0) and (20,0) TACNNTs, respectively. On the other hand, they are close to the LDA band gap of 1.99 eV for the g^t-C_3N_4 bilayer obtained in this work. They are also close to the PBE band gap of 2.00 eV previously reported.[23] Again, the gaps of the DWTACNNT are practically direct, because the valence bands are nearly flat.

Finally, we describe the effect of the P-doping on the various properties of (10,0)@(20,0) TACNNT, where the doping is supposed to occur on the outer shell. Table 3 shows that the interwall binding energy is affected little by the doping. The valence band and the conduction band still correspond to those of (20,0) and (10,0) TACNNT, respectively. More precisely, the valence band represents σ states concentrated on the P atom of (20,0) TACNNT. In Figures S4 and S5, the valence bands are located above other σ bands not concentrated on the atom. Consequently, the band gap decreases by a noticeable amount even at a quite low doping concentration. For example, Table 3 shows that the gaps decrease by more than 0.21 eV even when the P/N ratio is 1/120. As has been already noted for (14,0) TACNNT, Table 3 shows that the P_p^o-doping decrease the gap more than the P_g-doping.

4. CONCLUSIONS

In summary, we have theoretically investigated the possibility of forming TACNNTs from g^t-C_3N_4 sheets synthesized very recently. The nanotubes are different from heptazine-based nanotubes with the same stoichiometry, which has been a subject of many studies. In contrast to the case of SWCNTs, the negative strain energy indicates that SWTACNNTs are appreciably more stable than a single sheet of g^t-C_3N_4. This observation can be ascribed to the release of repulsion among lone-pair electrons of pyridinelike nitrogen atoms upon tube formation. In addition, the TACNNTs are chirality-specific: *z*TACNNTs are much more stable than *a*TACNNTs. Our PBE calculation shows that they are semiconductors with band gaps of ~2.60 eV. Specifically, (14,0) TACNNT is the most stable.

B-doping at carbon sites turns the SWTACNNT into a magnetic semiconductor, where spins of adjacent magnetic centers strongly couple ferromagnetically. The band gap of the minority spin is *significantly* smaller than that of the majority spin. Therefore, the *p*-magnetism of the B-doped TACNNT could be potentially useful for spintronic devices. P-doping at nitrogen sites decreases the band gap by more than 0.28 eV at the P/N concentration of 1/56. DWTACNNTs are appreciably more stable than constituent SWTACNNTs. In addition, they are significantly more stable than g^t-C_3N_4 bilayer, leading us to conjecture that multi-walled TACNNTs are highly possible. One of the best inner-outer pairs was found to be (10,0)@(20,0) TACNNT, for which the band gap is more than 0.48 eV smaller than those of constituent SWTACNNTs. P-doping on the outer shell of the DWTACNNT again decreases the band gap by an amount similar to that in the SWTACNNT. We believe that TACNNTs can be used for nanotransistors and optoelectronics, because the band gap corresponding to visible light can be tuned by various kinds of doping.

ACKNOWLEDGMENTS

This work was supported by the Basic Science Research Program through the National Research Foundation of Korea (NRF) funded by the Ministry of Education, Science and Technology (Grant 2012-R1A1A-2039084). We would also like to thank Jeonju University for partial financial support. Some of the computations were performed using a supercomputer of the Korea Institute of Science and Technology Information under contract No. KSC-2014-C2-001.

Notes

Electronic Supplementary Information (ESI) is available for Figures S1-S5.

References

1. D. M. Teter, R. J. Hemley, *Sicence*, 1996, **271**, 53.
2. Z. Ma, Z. Zhao, Q. Tang, Z. Zhou, *Int. J. Hydrogen Energ*., 2014, **39**, 5037.
3. S. Wang, C. Li, T. Wang, P. Zhang, A. Li, J. Gong, *J. Mater. Chem. A*, 2014, **2**, 2885.
4. L. Hultman, S. Stafstrom, Z. Czigany, J. Neidhardt, N. Hellgren, I. F. Brunell, K. Suenaga, C. Colliex, *Phys. Rev. Lett.*, 2001, **87**, 225503.
5. M. J. Bojdys, J.-O. Müller, M. Antonietti, A. Thomas, *Chem. Eur. J.*, 2008, **14**, 8177.
6. J. S. Lee, X. Wang, H. Luo, S. Dai, *Adv. Mater.*, 2010, **22**, 1004.
7. E. Krock, M. Schwarz, E. Horath-Bordon, P. Kroll, B. Noll, A. D. Norman, *New J. Chem.*, 2002, **26**, 508.
8. A. Thomas, A. Fischer, F. Goettmann, M. Antonietti, J.-O. Müller, R. Schlögl, J. M. Carlsson, *J. Mater. Chem.*, 2008, **18**, 4893.
9. Y. Wang, X. Wang, M. Antonietti, *Angew. Chem. Int. Ed.*, 2012, **51**, 68.
10. P. Zhang, Y. Wang, J. Yao, C. Wang, C. Yan, M. Antonietti, *Adv. Synth. Catal.* 2011, **353**, 1447.
11. P. Zhang, Y. Wang, J. Yao, H. Li, M. Antonietti, *Green Chem.* 2012, **14**, 1904.
12. X. Wang, S. Blecher, M. Antonietti, *ACS Catal.*, 2012, **2**, 1596.
13. P. Zhang, Y. Gong, H. Li, Z. Chen, Y. Wang, *RSC Adv*. 2013, **3**, 5121.
14. P. Zhang, H. Li, Y. Wang, *Chem. Commun*. 2013, **3**, 5121.
15. J. Wang, Z. Guan, J. Huang, Q. Li, J. Yang, *J. Mater. Chem. A*, 2014, **2**, 7960.
16. Y. Zheng, J. Liu, J. Liang, M. Jaroniec, S. Z. Qiao, *Energy Environ. Sci.*, 2012, **5**, 6717.
17. X. Zhang, X. Xie, H. Wang, J. Zhang, B. Pan, Y. Xie, *J. Am. Chem. Soc.*, 2013, **135**, 18.
18. S. Cao, J. Yu, *J. Phys. Chem. Lett.*, 2014, **5**, 2101.
19. S. C. Yan, Z. S. Li, Z. G. Zou, *Langmuir*, 2009, **25**, 10397.

20. J. Gao, Y. Zhou, Z. Li, S. Yan, N. Wang, Z. Zou, *Nanoscale*, 2012, **4**, 3687.

21. J. Li, C. Cao, H. Zhu, *Nanotechnology*, 2007, **18**, 115605.

22. J. Garcia, P. Kroll, *J. Mater. Chem.*, 2009, **19**, 3020.

23. G. Algara-Siller, N. Severin, S. Y. Chong, T. Björkman, R. G. Palgrave, A. Laybourn, M. Antonietti, Y. Z. Khimyak, A. V. Krasheninnikov, J. P. Rabe, U. Kaiser, A. I. Cooper, A. Thomas, M. J. Bojdys, *Angew. Chem. Int. Ed.*, 2014, **53**, 7450.

24. A. M. Enyashin, A. L. Ivanovskii, *Dokl. Phys. Chem.*, 2004, **398**, 211.

25. Q. X. Guo, Y. Xie, X. J. Wang, S. Y. Zhang, T. Hou, S. C. Lv, *Chem. Commun.*, 2004, 26.

26. G. Kresse, J. Hafner, *Phys. Rev. B*, 1993, **47**, 558.

27. G. Kresse, D. Joubert, *Phys. Rev. B*, 1999, **59**, 1758.

28. G. Kresse, J. Furthmüller, *Phys. Rev. B*, 1996, **54**, 11169.

29. S. J. Grimme, *Comput. Chem.*, 2006, **27**, 1787.

30. Y. Zhang, T. Mori, J. Ye, M. Antonietti, *J. Am. Chem. Soc.*, 2010, **132**, 6294–6295.

31. Y. Wang, Y.; H. Li, H.; J. Yao, J.; X. Wang, X.; M. Antoniettia, M. *Chem. Sci.*, 2011, 2, 446.

32. B. Shan, K. Cho, *Phys. Rev. B*, 2006, **73**, 081401.

Table 1. Various parameters for *a*TACNNTs of various chiral indices *n*: the lattice constant of a primitive cell (L), the distance between adjacent nitrogen atoms with lone pairs ($l_{N\text{-}N}$), inner and outer diameters (d), the strain energy (E_{st}), the band gap (E_g), and the direct gap (E_g^{direct}). For the band gap, the corresponding transition is also shown in a parenthesis.

(n,n)	L (Å)	$l_{N\text{-}N}$ (Å)[a]	d (Å)	E_{st} (eV/C_3N_4)	E_g (eV)	E_g^{direct} (eV)
(4,4)	4.78	2.45, 2.75, 2.75	4.64, 5.66	0.443	2.15(Γ→(Γ–X))	2.34(Γ→Γ)
(6,6)	4.70	2.53, 2.72, 2,69	6.62, 8.45	-0.041	2.62(Γ→ Γ)	2.62(Γ→ Γ)
(8,8)	4.69	2.54, 2.72, 2.62	9.21, 11.37	-0.156	2.64(Γ→(Γ–X))	2.67(Γ→Γ)
(10,10)	4.68	2.55, 2.68, 2.58	11.85, 13.50	-0.184	2.48 (Γ→X)	2.57(Γ→Γ)
(12,12)	4.68	2.54, 2.68, 2.56	15.14,16.46	-0.193	2.50 (Γ→X)	2.59(Γ→Γ)
(14,14)	4.68	2.54, 2.68, 2.54	17.69, 18.70	-0.199	2.62(Γ→X)	2.66(Γ→Γ)
(16,16)	4.68	2.52, 2.65, 2.53	19.65, 21.68	-0.172	2.51 (Γ→X)	2.59(Γ→Γ)

[a] Three numbers for $l_{N\text{-}N}$ correspond to N_p^{o1}-N_p^{i}, N_p^{o2}-N_p^{i} , and N_p^{o1}-N_p^{o2} distances, respectively, where N_p^{o1}, N_p^{o2} , and N_p^{i} are defined in Figure 2. The corresponding distances in g^t-C_3N_4 are (2.47, 2.63, 2.47) in Å unit.

Table 2. Various parameters for zTACNNTs of various chiral indices n: the lattice constant of a primitive cell (L), the distance between adjacent nitrogen atoms with lone pairs ($l_{N\text{-}N}$), inner and outer diameters (d), the strain energy (E_{st}), the band gap (E_g), and the direct gap (E_g^{direct}). For the band gap, the corresponding transition is also shown in a parenthesis.

(n,0)	L (Å)	$l_{N\text{-}N}$ (Å)	d (Å) [a]	E_{st} (eV/C_3N_4)	E_g (eV)	E_g^{direct} (eV)
(8,0)	7.78	2.63, 2.63, 2.94	4.79 ,6.97	-0.137	2.78(X→X)	2.78(X→X)
(10,0)	7.84	2.64, 2.64, 2.84	6.01 , 8.43	-0.276	2.87(X→X)	2.87(X→X)
(14,0)	7.95	2.63, 2.63, 2.71	9.21, 11.30	-0.333	2.81(X→Γ)	2.91(Γ→Γ)
(18, 0)	7.97	2.61, 2.61, 2.64	12.28, 14.35	-0.315	2.76 (X→Γ)	2.77(Γ→Γ)
(20,0)	8.00	2.62, 2.62, 2.61	13.98 ,15.83	-0.303	2.70(Γ→Γ)	2.70(Γ→Γ)
(24,0)	8.01	2.60, 2.60, 2.58	17.07, 18.81	-0.277	2.61(X→Γ)	2.62(Γ→Γ)
(28,0)	8.02	2.60, 260, 2.56	20.64, 21.86	-0.250	2.55(X→Γ)	2.56(Γ→Γ)

[a] Three numbers for $l_{N\text{-}N}$ correspond to N_p^{o1}-N_p^{i}, N_p^{o2}-N_p^{i} , and N_p^{o1}-N_p^{o2} distances, respectively, where N_p^{o1}, N_p^{o2} , and N_p^{i} are defined in Figure 3. The corresponding distances in g^t-C_3N_4 are (2.47, 2.63, 2.47) in Å unit.

Table 3. Interwall binding energies (E_b) per $(C_3N_4)_2$, the band gap (E_g), and the direct gap (E_g^{direct}) for pure and P-doped (10,0)@(20,0) TACNNT at P/N ratio of 1/120. For the band gap, the corresponding transition is also shown in a parenthesis.

Configuration	E_b(eV)		E_g (eV)	E_g^{direct} (eV)
	PBE-D2	LDA		
FF	-0.23	-0.15	2.13(Γ→Γ)	2.13(Γ→Γ)
RF	-0.24	-0.16	2.09(Γ→Γ)	2.09(Γ→Γ)
P_g-doped FF	-0.23	-0.15	1.90 (X→Γ)	1.94(X→X)
P_p^o-doped FF	-0.24	-0.15	1.78(X→Γ)	1.80(X→X)
P_g-doped RF	-0.24	-0.15	1.88(X→X)	1.88(X→X)
P_p^o-doped RF	-0.24	-0.16	1.83(X→Γ)	1.87(X→X)

Figures

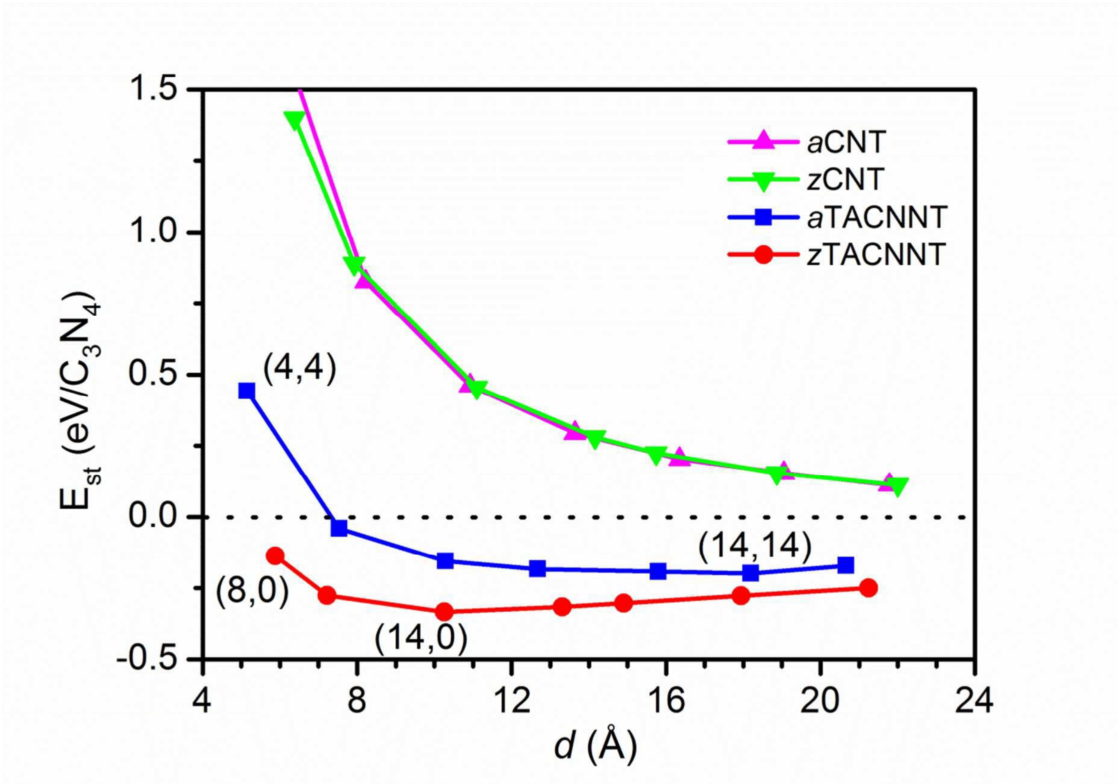

Figure 1. The strain energy (E_{st}) versus diameter (d) for TACNNTs and CNTs. For TACNNTs, the diameter is defined as the average value of inner and outer diameters shown in Tables 1 and 2. The chiral index is explicitly shown for the most stable one for each kind of tube.

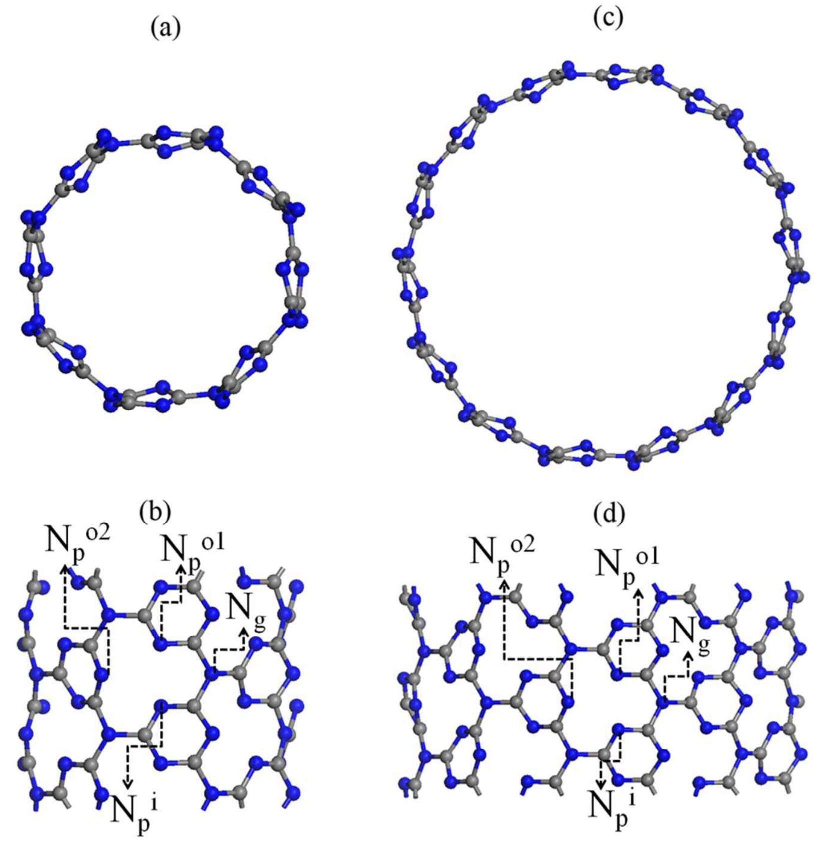

Figure 2. Structures of (8,8) (a,b) and (14,14) (c,d) TACNNTs viewed along the tube axis (X) and a direction (Z) perpendicular to it. Four kinds of nitrogen atoms around a vacancy site are also defined: N_g, N_p^{o1}, N_p^{o2} and N_p^{i}.

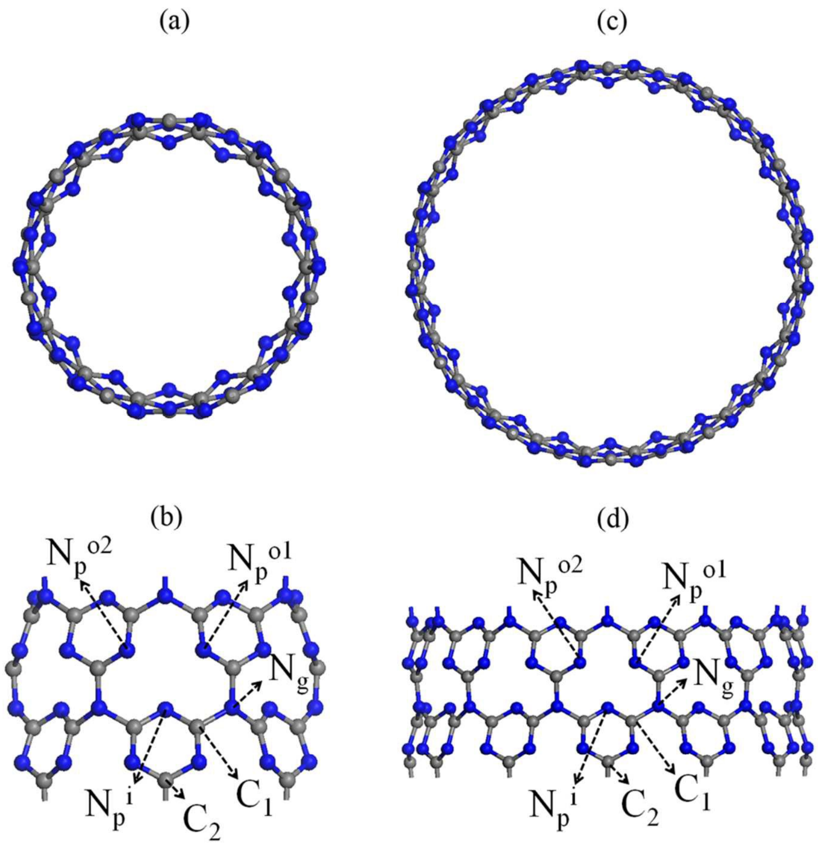

Figure 3. Structures of (14,0) (a,b) and (24,0) (c,d) TACNNTs viewed along the tube axis (X) and a direction (Z) perpendicular to it. Four kinds of nitrogen atoms around a vacancy site are also defined: N_g, N_p^{o1}, N_p^{o2} and N_p^{i}. Two kinds of carbon atoms, C_1 and C_2, are also defined.

(a)

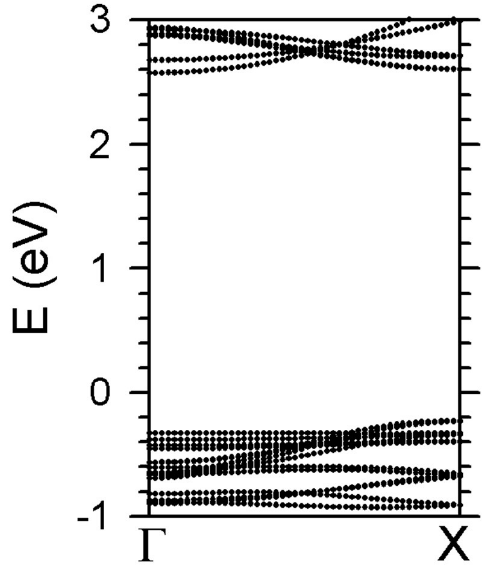

(b)

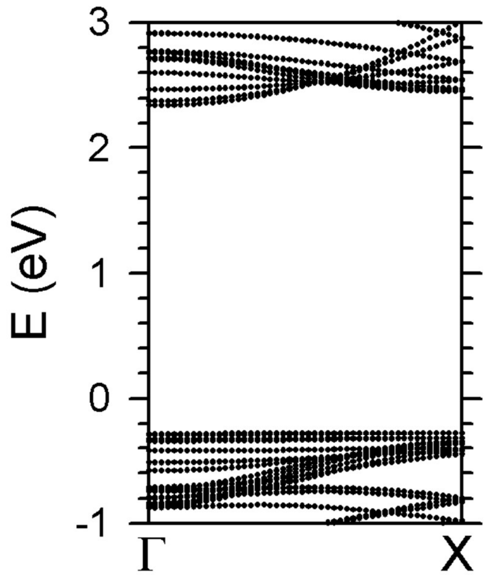

Figure 4. The band structures of (14,0) (a) and (24,0) (b) TACNNTs.

(a)

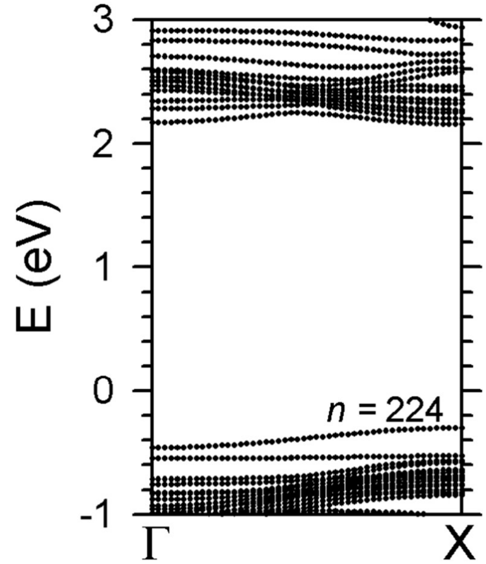

(b)

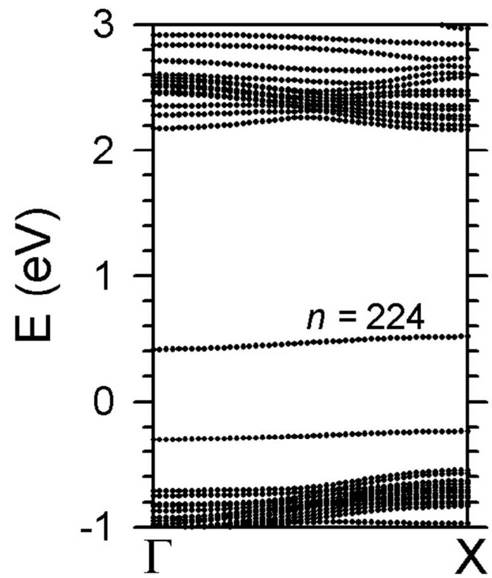

Figure 5. The band structure of (14,0) TACNNT doped with a B_{C1} atom at a C_1 site shown in Figure 3 for majority (a) and minority spins (b).

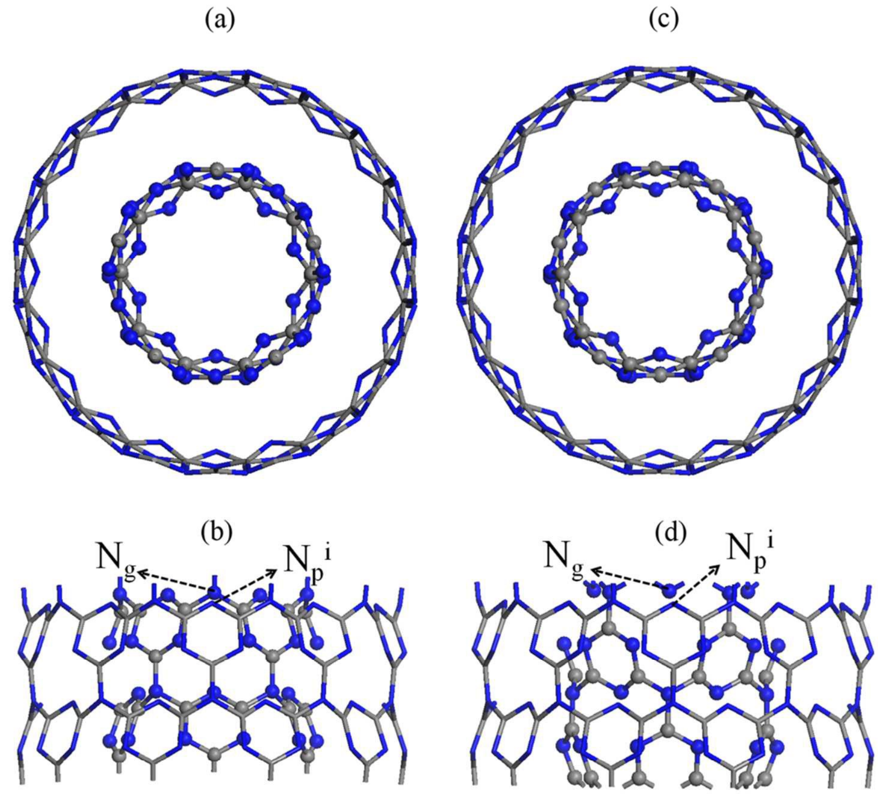

Figure 6. The geometrical structures of FF (a,b) and FR (c,d) configurations for (10,0)@(20,0) DWTACNNT. Inner and outer shells are represented by ball-and-stick and stick models, respectively. The N_g atom of the inner shell and N_p^i atom of the outer shell are also shown.

(a)

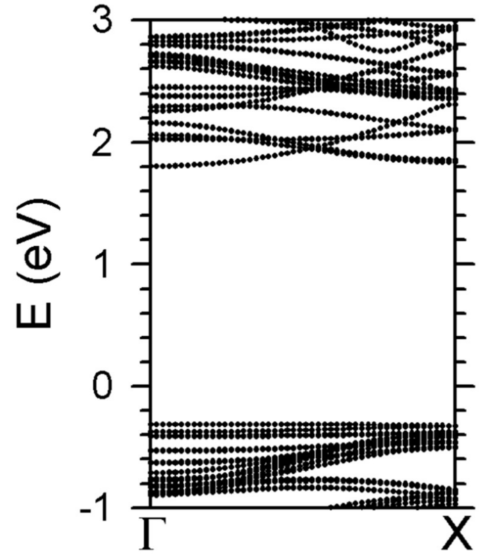

(b)

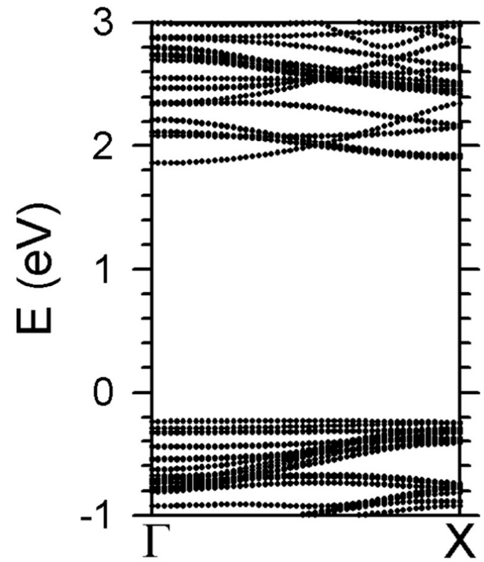

Figure 7. The band structures of FF (a) and FR (b) configurations for (10,0)@(20,0) DWTACNNT.

TOC Figure

In contrast to the case of carbon nanotubes, the negative strain energy indicates that single-walled and double-walled triazine-based carbon nitride nanotubes (TACNNTs) are appreciably more stable than the single layer and the bilayer of g^t-C_3N_4, respectively. The band gap of (10,0)@(20,0) TACNNTs is appreciably smaller than those of constituent SWCNNTs. Boron-doping turns the material into a magnetic semiconductor.